

A hadron-quark hybrid model reliable for the EoS in $\mu_B \leq 400$ MeV

Akihisa Miyahara,^{1,*} Masahiro Ishii,^{2,†} Hiroaki Kouno,^{3,‡} and Masanobu Yahiro^{2,§}

¹Observation Division, Chubu aviation weather service center,
Japan Meteorological Agency, Tokoname 479-0881, Japan

²Department of Physics, Graduate School of Sciences, Kyushu University, Fukuoka 819-0395, Japan

³Department of Physics, Saga University, Saga 840-8502, Japan

(Dated: July 18, 2019)

We present a simple version of hadron-quark hybrid (HQP) model. The model is composed of the simple independent quark model for QGP states and an improved version of volume-excluded HRG model for hadronic states. The improved version of volume-excluded HRG model yields the pressure as a simple analytic form. The switching function from hadron states to QGP states in the present model has no chemical potential dependence. The present HQP model with the simple switching function is successful in reproducing the Polyakov loop at zero chemical potential and the EoS in $\mu_B \leq 400$ MeV.

PACS numbers: 11.30.Rd, 12.40.-y, 21.65.Qr, 25.75.Nq

I. INTRODUCTION

Lattice QCD (LQCD) provides a lot of information on hot QCD. In particular, the recent 2+1-flavor LQCD simulation [1] has confirmed that the chiral and the deconfinement transition are “crossover” at finite temperature (T) and zero baryon chemical potential ($\mu_B = 0$), where the continuum and thermodynamic limits were carefully taken. In general, such crossover nature means that the chiral and the deconfinement transition are not completely decoupled and the transition temperatures depends on the choice of observables. In fact, observable-dependent transition temperatures $T_c^{(O)}(\mu_B)$ have been discussed in LQCD simulations for zero and small μ_B ; actually, the renormalized chiral condensate $O = \Delta_{l,s}(T, \mu_B)$, the Polyakov loop $O = \Phi(T, \mu_B)$, the energy density $O = \varepsilon(T, \mu_B)$ and the trace anomaly $O = I(T, \mu_B)$ are taken in Refs. [2–9]. The definition and the determination are essential for the investigation of the presence or absence of critical endpoint (CEP) in QCD phase diagram. Particularly in Ref. [9], the LQCD data disfavors the existence of the CEP in $\mu_B/T \leq 2$ and $T/T_c^{(\Delta_{l,s})}(\mu_B = 0) > 0.9$. Another important subject is to understand LQCD data on T dependence of the equation of state (EoS), especially for the crossover region ($100 \text{ MeV} \leq T \leq 400 \text{ MeV}$). In the region, hadrons are supposed to melt into the strongly-correlated quark-gluon plasma; however, the physical interpretation of such hadron-quark transition has not been established yet. The EoS including the hadron-quark transition is necessary for the analyses of relativistic nuclear collisions. For these reasons, a lot of QCD data have been accumulated [1–13].

As a complementary approach to LQCD simulations, we can consider effective models. This approach is useful for the prediction of the transition lines, the existence and the location of the CEP, and the EoS. In fact, a lot of predictions are

made for these quantities. The hadron resonance gas (HRG) model is a simple model for hadronic matter. The hadron is treated as non-interacting gas, and all hadrons listed in Particle Data Book [14] are taken into account in the model. The HRG model remarkably reproduces LQCD data on the various thermodynamic quantities in $T \lesssim 1.3T_c^{(\Delta_{l,s})}(\mu_B = 0)$ [11], which indicates that one cannot neglect the excited hadrons even above the chiral transition temperature and hence hadrons possibly coexistent with quarks and gluons. The simultaneous treatment of quarks and hadrons has been discussed for a long time. The various models have been proposed so far, such as the quark-meson model [15] and the Nambu–Jona-Lasinio (NJL) model with mesonic loops, quark-diquark coupling and chiral soliton. However, excited hadrons are absent in such models.

In our previous papers [20, 21], we proposed the hadron-quark hybrid (HQP) model in order to describe the coexistence of quarks and hadrons. In the model, the total entropy $s(T, \mu_B)$ is divided into hadron and quark pieces: Namely,

$$s(T, \mu_B) = f_H(T, \mu_B)s_H(T, \mu_B) + [1 - f_H(T, \mu_B)]s_Q(T, \mu_B), \quad (1)$$

where the function s_H (s_Q) is the entropy density for hadronic matter (quark–gluon plasma). The weight function f_H means the occupancy of hadronic matter in the total entropy and is constrained in $0 \leq f_H \leq 1$. The $s(T, \mu_B)$ was determined from LQCD data on T dependence of s_{LQCD} and the second-order susceptibilities at $\mu_B = 0$. We apply HRG model for s_H and independent-quark (IQ) model for s_Q . The IQ model is a simplified version of Polyakov-loop extended Nambu–Jona-Lainio (PNJL) model [22–25], that is, this model treats the coupling between the quark field and the homogeneous classical gauge field, but not the couplings between quarks. The neglect of quark-quark interactions are justified from the fact that the light-quark chiral condensate is quite small in $T \gtrsim 220 \text{ MeV}$ where $s_Q > s_H$. In our previous version of HQP model [20, 21], we have confirmed that the HQP model well describe the LQCD data on the EoS for both $T \leq T_c$ and $T \geq T_c$ [16–21].

As another advantage of our approach, s_{LQCD} automati-

*miyahara@email.phys.kyushu-u.ac.jp

†ishii@phys.kyushu-u.ac.jp

‡kounoh@cc.saga-u.ac.jp

§orion093g@gmail.com

cally satisfies the thermodynamic inequality and the Nernst's theorem [26],

$$\left. \frac{\partial s(T, \mu_B)}{\partial T} \right|_{\mu_B=0} > 0, \quad s(T, \mu_B)|_{T=\mu_B=0} = 0. \quad (2)$$

In the HRG model, the interactions between baryons (anti-baryon) are neglected, but it should be taken into account for μ_B dependence of thermodynamic quantities. A simple way of treating volume-exclusion effects (repulsive force) [27] was suggested in Refs. [28, 29]. This model is called “excluded-volume HRG (EV-HRG) model”. Furthermore, a method of treating an attractive force in addition to the repulsive force was proposed in Ref. [30]. The volume-exclusion effects are included by fitting the volume $b = 4 \cdot 4\pi r^3/3$ [26] to either LQCD data or the core radius r of nucleon-nucleon force [28, 29]. In the framework of Refs. [28–30], the interaction between baryon and anti-baryon and the radius of meson are neglected.

In this paper, we improve the HQH model of Ref. [21], taking the EV-HRG model for the hadron piece and using the simple IQ model for the quark-gluon piece. The EV-HRG model taken yields the pressure as a simple analytic function and guarantees that the pressure is μ_B even. We refer to the present version of HQH model as “simple HQH (sHQH) model”.

The switching function f_H is determined from s_{LQCD} at $\mu_B = 0$, i.e., f_H has no μ_B dependence. The sHQH model with the switching function well accounts for the Polyakov loop at zero chemical potential and the EoS in $\mu_B \leq 400$ MeV, without introducing μ_B dependence to f_H , where the core radius $r = 0.335$ fm is taken.

The $\Delta_{1,s}$ and the Φ signal the chiral and the deconfinement transition, respectively. The $\Delta_{1,s}$ calculated with the HRG model becomes negative in higher T [5], whereas the corresponding LQCD result is positive. The present model has the same problem. As an interesting result of LQCD simulations in Ref. [5], the peak position of $d\Delta_{1,s}/dT$ agrees with that of $d\varepsilon/dT$ at $\mu_B = 0$. In Ref. [7], furthermore, the transition line is estimated by the peak of $d\varepsilon/dT$ for finite μ_B . Therefore, we use the peak and the half-value width of $d\varepsilon/dT$ as a transition region in μ_B - T plane. We guess that the transition region determined from ε is close to the chiral-transition region calculated with LQCD simulations [8]. As a result, we show that both the regions are close to each other in $\mu_B \leq 400$ MeV.

As a deconfinement-transition region, we take the peak and the half-value width of $d\Phi/dT$ and predict the transition region for $\mu_B \leq 400$ MeV. We also determine a transition line from isentropic trajectories, and show that the transition line is between the deconfinement line and the transition line determined from ε .

This paper is organized as follows. In Sec. II, we show the model building. Numerical results are shown in Sec III. Section IV is devoted to a summary.

II. MODEL BUILDING

We improve the HQH model of Ref. [21], modifying the EV-HRG model for the hadron part and taking the IQ mode for the quark-gluon one.

For the 2+1 flavor system, we can consider the chemical potentials of u, d, s quarks by μ_u, μ_d, μ_s , respectively. These potentials are related to the baryon-number (B) chemical potential μ_B , the isospin (I) chemical potential μ_I and the hypercharge (Y) chemical potential μ_Y as

$$\begin{aligned} \mu_B &= \mu_u + \mu_d + \mu_s, \\ \mu_I &= \mu_u - \mu_d, \\ \mu_Y &= \frac{1}{2}(\mu_u + \mu_d - 2\mu_s). \end{aligned} \quad (3)$$

As for μ_I and μ_Y , the right-hand side of Eq. (3) comes from the diagonal elements of the matrix representation of Cartan algebra in $SU(3)$ group: $\mu_I = (1, -1, 0)(\mu_u, \mu_d, \mu_s)^t$ and $\mu_Y = (1/2)(1, 1, -2)(\mu_u, \mu_d, \mu_s)^t$. Equation (3) yields

$$\begin{aligned} \mu_u &= \frac{1}{3}\mu_B + \frac{1}{2}\mu_I + \frac{1}{3}\mu_Y, \\ \mu_d &= \frac{1}{3}\mu_B - \frac{1}{2}\mu_I + \frac{1}{3}\mu_Y, \\ \mu_s &= \frac{1}{3}\mu_B - \frac{2}{3}\mu_Y. \end{aligned} \quad (4)$$

A. HRG model

For later convenience, we start with the HRG model. In the model, the pressure P_H is divided into the baryon (B) part P_B , the anti-baryon (aB) part P_{aB} and the meson (M) part P_M :

$$P_H \equiv P_B + P_{aB} + P_M \quad (5)$$

with

$$P_B = \sum_{i \in B} d_i T \int \log(1 + e^{-(E_{B,i} - \mu_{B,i})/T}), \quad (6)$$

$$P_{aB} = \sum_{i \in aB} d_i T \int \log(1 + e^{-(E_{B,i} + \mu_{B,i})/T}), \quad (7)$$

$$\begin{aligned} P_M &= - \sum_{j \in \text{Meson}} d_j T \int \{ \log(1 - e^{-(E_{M,j} - \mu_{M,j})/T}) \\ &\quad + \log(1 - e^{-(E_{M,j} + \mu_{M,j})/T}) \} \end{aligned} \quad (8)$$

for $E_{B,i} = \sqrt{\mathbf{p}^2 + m_{B,i}^2}$ and $E_{M,j} = \sqrt{\mathbf{p}^2 + m_{M,j}^2}$, where $m_{B,i}$ ($m_{M,j}$) and μ_i (μ_j) is the mass and the chemical potential of the i -th baryon (j -th meson), respectively. Here we have used the shorthand notation

$$\int \equiv \int \frac{d^3 \mathbf{p}}{(2\pi)^3}. \quad (9)$$

for the integration over 3d-momentum \mathbf{p} . In Eq. (5), all the hadrons listed in the Particle Data Table [14] are taken.

B. Modified version of EV-HRG

We first explain the EV-HRG model of Refs. [28–30]. The pressure $P_{\text{EV;H}}$ is obtained by

$$P_{\text{EV;H}} = P_{\text{EV;B}} + P_{\text{EV;aB}} + P_{\text{M}} \quad (10)$$

with

$$P_{\text{EV;B}} = \sum_{i \in \text{B}} d_i T \int \log(1 + e^{-(E_{\text{B},i} - \mu_{\text{EV;B},i})/T}), \quad (11)$$

$$P_{\text{EV;aB}} = \sum_{i \in \text{aB}} d_i T \int \log(1 + e^{-(E_{\text{B},i} + \mu_{\text{EV;aB},i})/T}). \quad (12)$$

Here the effective baryon and anti-baryon chemical potentials, $\mu_{\text{EV;B},i}$ and $\mu_{\text{EV;aB},i}$, are defined by

$$\mu_{\text{EV;B},i}/T = \mu_{\text{B},i}/T - \bar{b} P_{\text{EV;B}}/T^4, \quad (13)$$

$$\mu_{\text{EV;aB},i}/T = \mu_{\text{B},i}/T - \bar{b} P_{\text{EV;aB}}/T^4, \quad (14)$$

where $\bar{b} = bT^3$ for a positive volume parameter b . It is not easy to obtain $P_{\text{EV;B}}$ and $P_{\text{EV;aB}}$, since $\mu_{\text{EV;B},i}$ ($\mu_{\text{EV;aB},i}$) includes $P_{\text{EV;B}}$ ($P_{\text{EV;aB}}$). Actually, $P_{\text{EV;B}}$ and $P_{\text{EV;aB}}$ are obtained by solving Eqs. (11) and (12) numerically.

In QCD, the pressure is charge-conjugation even (μ_{B} even). Hence the $P_{\text{EV;H}}$ should be μ_{B} even, because it is a model of explaining QCD in $T < T_c$. However, $\mu_{\text{EV;B},i}$ includes a μ_{B} -odd term μ_{B} and a μ_{B} -even term $\bar{b} P_{\text{EV;B}}/T^4$, so that $P_{\text{EV;H}}$ is not μ_{B} even.

The $P_{\text{EV;B}}$ and $P_{\text{EV;aB}}$ are now modified as

$$P_{\text{mod;B}} = \sum_{i \in \text{B}} d_i T \int \log(1 + e^{-(E_{\text{B},i} - \mu_{\text{mod;B},i})/T}), \quad (15)$$

$$P_{\text{mod;aB}} = \sum_{i \in \text{aB}} d_i T \int \log(1 + e^{-(E_{\text{B},i} + \mu_{\text{mod;aB},i})/T}). \quad (16)$$

with

$$\mu_{\text{mod;B},i}/T = \mu_{\text{B},i}/T - \bar{b} P_{\text{mod;B}}/T^4, \quad (17)$$

$$\mu_{\text{mod;aB},i}/T = \mu_{\text{B},i}/T + \bar{b} P_{\text{mod;aB}}/T^4, \quad (18)$$

The sum of $P_{\text{mod;B}}$ and $P_{\text{mod;aB}}$ are μ_{B} even, since the sum is invariant under $\mu_{\text{B}} \rightarrow -\mu_{\text{B}}$. For this reason, we take Eqs. (15)–(18). These equations show that $P_{\text{B}} \geq P_{\text{aB}}$.

The $P_{\text{mod;B}}$ and $P_{\text{mod;aB}}$ can be rewritten into

$$\begin{aligned} \frac{P_{\text{mod;B}}}{T^4} &= \sum_{i \in \text{B}} A_i \sum_{\ell=1}^{\infty} \frac{(-1)^{\ell+1}}{\ell^2} \\ &\times K_2\left(\frac{\ell m_i}{T}\right) \exp\left(\frac{\ell \mu_{\text{mod;B},i}}{T}\right), \end{aligned} \quad (19)$$

$$\begin{aligned} \frac{P_{\text{mod;aB}}}{T^4} &= \sum_{i \in \text{aB}} A_i \sum_{\ell=1}^{\infty} \frac{(-1)^{\ell+1}}{\ell^2} \\ &\times K_2\left(\frac{\ell m_i}{T}\right) \exp\left(-\frac{\ell \mu_{\text{mod;aB},i}}{T}\right) \end{aligned} \quad (20)$$

for

$$A_i \equiv \frac{d_i}{2\pi} \left(\frac{m_i}{T}\right)^2. \quad (21)$$

LQCD data on the EoS are available for $T \leq 400$ MeV and $\mu_{\text{B}} \leq 400$ MeV [5, 7]. We then consider this region. We consider P_{B} , because of $P_{\text{B}} \geq P_{\text{aB}}$. The ℓ convergence of Eq. (19) becomes worse as $|(\mu_{\text{B}} - m_i)/T|$ becomes larger; note that $K_2(x)$ is proportional to $\exp(-x)$ for large x and $\mu_{\text{B}} - m_i$ is negative. Therefore, the convergence is worst for the smallest case $(939-400)/400$ where $T = \mu_{\text{B}} = 400$ MeV and $m_N = 939$ MeV. Taking the $\ell = 1$ term only is a 3 % error in Eqs. (19). In actual calculations, nucleon contribution in P_{B} is only 3 %, so that taking the $\ell = 1$ term only corresponds to 0.1% error. We can identify P_{B} with its $\ell = 1$ term and P_{aB} with its $\ell = 1$ one. This approximation is called “ $\ell = 1$ identification in this paper

Using the $\ell = 1$ identification, we can rewrite $P_{\text{mod;B}}$ as

$$\frac{P_{\text{mod;B}}}{T^4} = \sum_{i \in \text{B}} A_i K_2\left(\frac{m_i}{T}\right) \exp\left(\frac{\mu_{\text{mod;B},i}}{T}\right), \quad (22)$$

Multiplying both the sides of Eq. (22) by $\bar{b} \exp(\bar{b} P_{\text{mod;B}}/T^4)$ and using the $\ell = 1$ identification, one can obtain

$$\begin{aligned} &\bar{b} \frac{P_{\text{mod;B}}}{T^4} \exp\left(\bar{b} \frac{P_{\text{mod;B}}}{T^4}\right) \\ &= \bar{b} \sum_{i \in \text{B}} A_i K_2\left(\frac{m_i}{T}\right) \exp\left(\frac{\mu_{\text{B},i}}{T}\right) \\ &= \bar{b} \sum_{i \in \text{B}} A_i \sum_{\ell=1}^{\infty} \frac{(-1)^{\ell+1}}{\ell^2} K_2\left(\frac{\ell m_i}{T}\right) \exp\left(\frac{\ell \mu_{\text{B},i}}{T}\right) \\ &= \bar{b} \frac{P_{\text{mod;B}}}{T^4}, \end{aligned} \quad (23)$$

Noting that the Lambert $W(z)$ function is the inverse function of $We^W = z$, one can get $P_{\text{mod;B}}$ as a simple analytic function: Namely,

$$\frac{P_{\text{mod;B}}}{T^4} = \frac{W(\bar{b} P_{\text{mod;B}}/T^4)}{\bar{b}}. \quad (24)$$

In the limit of $\bar{b} = 0$, the $P_{\text{mod;B}}$ tends to P_{B} , because of $W(z) \rightarrow z$. Parallel discussion is possible for anti-baryon. The result is

$$\frac{P_{\text{mod;aB}}}{T^4} = \frac{W(\bar{b} P_{\text{aB}}/T^4)}{\bar{b}}. \quad (25)$$

Hence the hadronic pressure becomes

$$P_{\text{mod;H}} = P_{\text{mod;B}} + P_{\text{mod;aB}} + P_{\text{M}} \quad (26)$$

with Eqs. (24) and (25). The entropy density $s_{\text{mod;H}}$ is obtained from $P_{\text{mod;H}}$ as

$$s_{\text{mod;H}} = \frac{\partial P_{\text{mod;H}}}{\partial T}. \quad (27)$$

This modified version of EV-HRG model is referred to as “modified EV-HRG model”.

Figure 1 shows T dependence of the total pressure $P(T)$ for $\mu_B = 0, 400$ MeV. The results of modified EV-HRG and HRG models are compared with LQCD ones [13]. In the modified EV-HRG model, we take the core radius 0.335 fm as a value of r , i.e., $b = 0.64$ fm³. For $\mu_B = 400$ MeV (lower panel), the EV-HRG result (solid line) agrees with LQCD one [13] in $T \lesssim 210$ MeV, while the HRG result (dashed line) is consistent with LQCD one in $T \lesssim 150$ MeV. For $\mu_B = 0$ MeV (upper panel), both the EV-HRG and the HRG result are consistent with LQCD one [13] in $T \lesssim 210$ MeV.

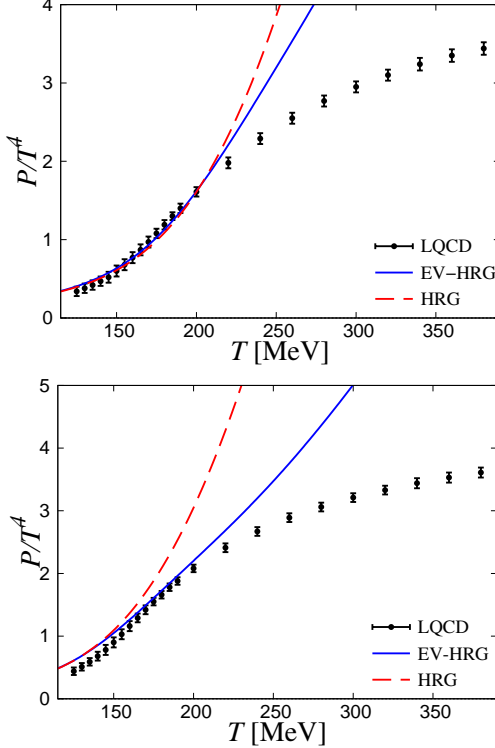


Fig. 1: T dependence of pressure P at $\mu_B = 0$ MeV (upper panel) and $\mu_B = 400$ MeV (lower panel). The solid and dashed lines stand for the results of modified EV-HRG model and HRG model, respectively. LQCD data are taken from Ref. [13].

C. Independent quark model

We have to consider QGP states in the region $T \gtrsim 200$ MeV by using the simple IQ model, since $f_H(T) < 1$, as shown later in Fig. 2. The Lagrangian density of the IQ model is

$$\mathcal{L}_Q = \sum_f \{ \bar{q}_f (i\gamma^\mu D_\mu - m_f) q_f \} - \mathcal{U}(T, \Phi, \bar{\Phi}), \quad (28)$$

where m_f is the current mass of f quark and $D_\mu = \partial_\mu - igA_\mu^a \frac{\lambda_a}{2} \delta^{\mu 0}$ with the Gell-Mann matrix λ_a in color space. See Refs. [24, 25] for the definition of the Polyakov loop Φ and its conjugate $\bar{\Phi}$.

Making the path integral over quark fields leads to

$$P_Q = -\mathcal{U}(T, \Phi, \bar{\Phi}) + 2 \sum_f \left[\int (T \log z_f^+ + T \log z_f^-) \right], \quad (29)$$

where

$$z_f^+ = 1 + 3\bar{\Phi}e^{-(E_f + \mu_f)/T} + 3\Phi e^{-2(E_f + \mu_f)/T} + e^{-3(E_f + \mu_f)/T}, \quad (30)$$

$$z_f^- = 1 + 3\Phi e^{-(E_f - \mu_f)/T} + 3\bar{\Phi} e^{-2(E_f - \mu_f)/T} + e^{-3(E_f - \mu_f)/T} \quad (31)$$

with $E_f = \sqrt{\mathbf{p}^2 + m_f^2}$. In Eq. (29), the vacuum term has been omitted, since the pressure calculated with LQCD simulations does not include the term. The Φ and $\bar{\Phi}$ are obtained by minimizing $\Omega_Q = -P_Q$.

The entropy density s_Q is obtained from P_Q as

$$s_Q = \frac{\partial P_Q}{\partial T}. \quad (32)$$

We take the Polyakov-loop potential of Ref. [21]:

$$\frac{\mathcal{U}(T, \Phi, \bar{\Phi})}{T^4} = -\frac{a(T)}{2} \Phi \bar{\Phi} + b(T) \log \{ 1 - 6\Phi \bar{\Phi} + 4(\Phi^3 + \bar{\Phi}^3) - 3(\Phi \bar{\Phi})^2 \}; \quad (33)$$

$$a(T) = a_0 + a_1 \left(\frac{T_0}{T} \right) + a_2 \left(\frac{T_0}{T} \right)^2, \quad (34)$$

$$b(T) = b_3 \left(\frac{T_0}{T} \right)^3. \quad (35)$$

The parameters a_0, a_1, a_2, b_3 and T_0 were fitted to 2+1 flavor s_{LQCD} in $400 \leq T \leq 500$ MeV; see Fig. 1 of Ref. [21] for the fit. The resulting values are tabulated in Table I.

TABLE I: Parameters in the Polyakov-loop potential.

a_0	a_1	a_2	b_3	T_0
2.457	-2.47	15.2	-1.75	270[MeV]

D. sHQH model

The total entropy reads

$$s(T, \mu_B) = f_H(T) s_{\text{mod:H}}(T, \mu_B) + [1 - f_H(T)] s_Q(T, \mu_B) \quad (36)$$

in the sHQH model, where it is assumed that the $f_H(T)$ has no chemical-potential dependence. Note that $s_{\text{mod:H}}$ and s_Q have chemical-potential dependence. Therefore, $f_H(T)$ is determined so as to $s = s_{\text{LQCD}}$ [13] at $\mu_B = 0$: Namely,

$$f_H(T) = \frac{s_{\text{LQCD}}(T) - s_Q(T)}{s_{\text{mod:H}}(T) - s_Q(T)}. \quad (37)$$

In Fig. 2, the $f_H(T)$ of Eq. (37) is shown by dots with error bars. The errors come from s_{LQCD} . The solid line is a fitting function for the $f_H(T)$ of Eq. (37); in the χ^2 fitting, the line is assumed to be 1 in $T < 180$ MeV. From now on, we regard the solid line as the switching function $f_H(T)$.

The pressure P with no vacuum contribution is obtainable from s_{LQCD} of Eq. (36):

$$P(T, \mu_B) = \int_0^T dT' s(T', \mu_B) \quad (38)$$

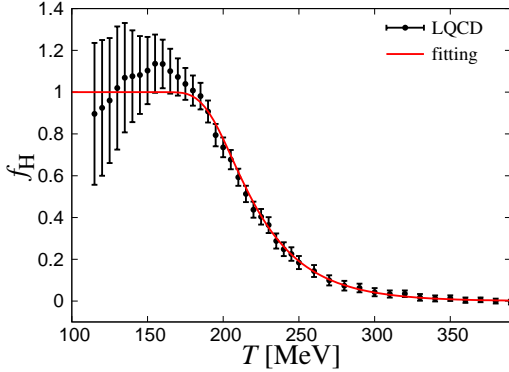


Fig. 2: T dependence of the switching function $f_H(T)$. The dots with error bars are the $f_H(T)$ of Eq. (37), The solid line is a fitting function for the $f_H(T)$; see the text for the fitting.

III. NUMERICAL RESULTS

As mentioned in Sec. I, we consider the transition region determined from with the peak and the half-value width of $d\varepsilon(T, \mu_B)/dT$ and the deconfinement-transition region with the peak and the half-value width of $d\Phi(T, \mu_B)/dT$.

A. T dependence of the Polyakov loop for $\mu_B = 0 \sim 400$ MeV

Figure 3 shows the Polyakov loop Φ as a function of T for the cases of $\mu_B = 0, 100, 200, 300, 400$ MeV. The LQCD result is available only for $\mu_B = 0$ MeV [5]. In the upper panel for $\mu_B = 0$ MeV, the sHQH result (solid line) well reproduces LQCD one in which the continuum limit is taken. We then predict the Φ for $\mu_B = 100, 200, 300, 400$ MeV in the lower panel. μ_B dependence of Φ is small.

B. Transitions

We first consider the case of $\mu_B = 0$. Table II shows results of sHQH model for the transition region T_c^ε determined from the peak and the half-valued width of $d\varepsilon(T, \mu_B)/dT$ and the deconfinement-transition region T_c^d deduced from $d\Phi(T, \mu_B)/dT$. The results are compared with LQCD data [5] on the chiral transition temperature $T_c^{X:LQCD}$ and the deconfinement temperature $T_c^{d:LQCD}$. One can see that

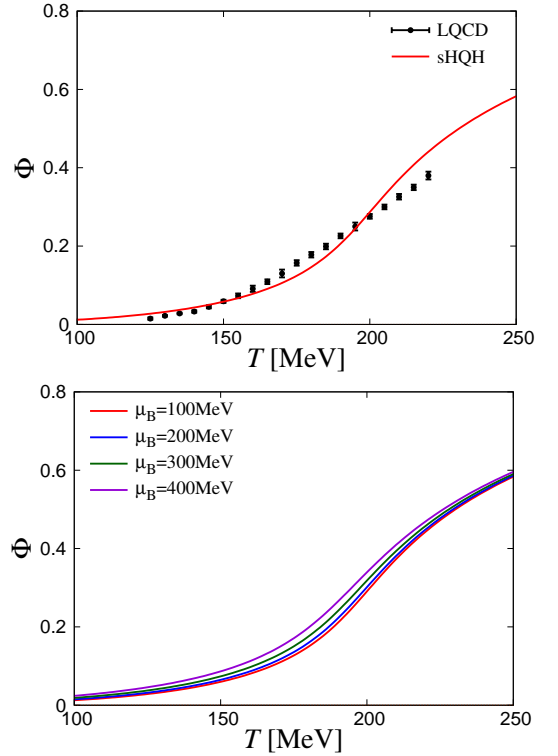


Fig. 3: T dependence of the Polyakov loop Φ . The upper panel is for $\mu_B = 0$ MeV and the lower panel is for $\mu_B = 100, 200, 300, 400$ MeV. The sHQH model results are shown by the solid lines. In the lower panel, four line correspond to the cases of $\mu_B = 100, 200, 300, 400$ MeV from right to left. LQCD data are taken from Ref. [5].

$T_c^{\Delta_{l,s}:LQCD}$ is included in the region T_c^ε , while T_c^d is consistent with $T_c^{d:LQCD}$.

T_c^ε	$T_c^{\Delta_{l,s}:LQCD}$	T_c^d	$T_c^{d:LQCD}$
137–204[MeV]	157(4)(3)[MeV]	177–239[MeV]	170±7[MeV]

TABLE II: Comparison between lattice transition temperatures and transition regions calculated with sHQH model for $\mu_B = 0$.

Figure 4 shows the transition region T_c^ε determined from the peak and the half-valued width of $d\varepsilon(T, \mu_B)/dT$ and the lattice chiral-transition region in μ_B - T plane; the former is calculated with the sHQH model and the latter is analytic continuation of LQCD simulations from imaginary to real μ [8]. The transition region determined from $d\varepsilon(T, \mu_B)/dT$ is shown by a horizontal line with cross for each of $\mu_B = 0, 100, 200, 300, 400$ MeV; the cross is a maximum value of $d\varepsilon/dT$ and the line means the half-value width of $d\varepsilon/dT$. The red solid line is made by connecting the crosses. Meanwhile, the blue band indicates the width of the chiral-transition region extrapolated from the imaginary- μ_B region [8]. The model result is consistent with the LQCD result.

Figure 5 shows the deconfinement-transition region in μ_B - T plane. The shah result is shown by a horizontal line with cross for each of $\mu_B = 0, 100, 200, 300, 400$ MeV. The solid line made by connecting the points stands for the

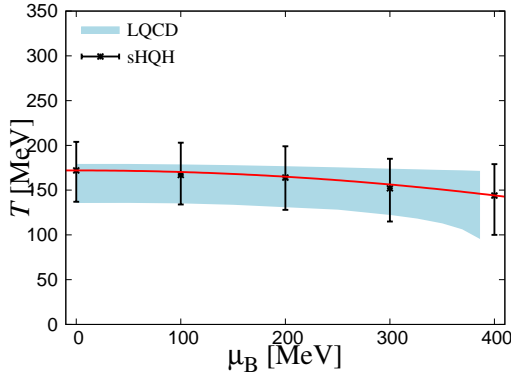


Fig. 4: The transition line determined from $d\varepsilon/dT$ in μ_B - T plane. The horizontal line with cross stands for the transition region determined from $d\varepsilon/dT$ and is calculated with the sHQH model. The transition line (red solid line), obtained by connecting the crosses, is expressed by $T = 172(1 - 0.03(\mu_B/172)^2)$ MeV. The blue band is the chiral-transition region determined by analytic continuation of LQCD simulations from imaginary to real μ [8].

deconfinement-transition line. μ_B dependence of the half-value width does not become large.

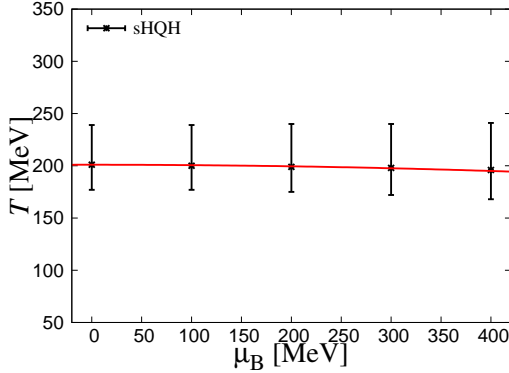


Fig. 5: Deconfinement-transition region in μ_B - T plane. See the text for the definition of lines. The deconfinement-transition line is $T = 201(1 - 0.0075(\mu_B/201)^2)$ MeV.

In Fig. 6, the solid curve is a line connecting the points at which the curvature of isentropic trajectory becomes maximum. This figure suggests that a transition line can be estimated by n/s in μ_B - T plane. Hence, the transition calculated with n/s may be deduced from relativistic nuclear collisions. There is no evidence of attractor of isentropic trajectory in the sHQH model.

In Fig. 7, the transition line calculated with n/s (dashed line) is compared with the transition line determined from $d\varepsilon/dT$ (dotted line) and the deconfinement-transition line (solid line). The transition line determined from n/s lies between the dotted and solid lines.

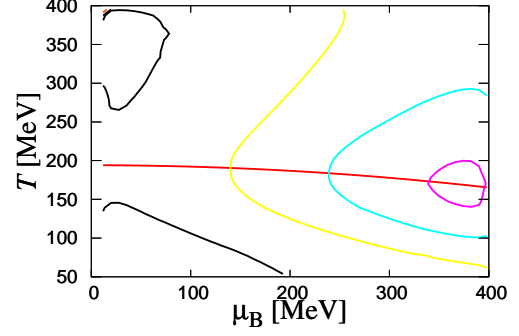


Fig. 6: Isentropic trajectories, $n/s=\text{const}$, in μ_B - T plane. The solid curve is a line connecting the points at which the curve of trajectory becomes maximum; the resulting curve is $T = 194(1 - 0.035(\mu_B/194)^2)$ MeV. The isentropic trajectories are shown by $n/s = 0.010, 0.015, 0.020, 0.025$ from left to right.

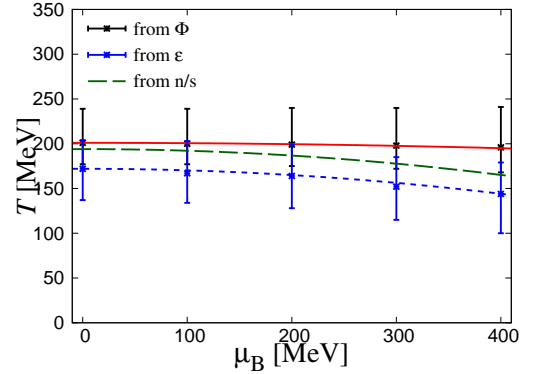


Fig. 7: Transition lines in μ_B - T plane. The chiral-transition line determined from ε is $T = 172(1 - 0.03(\mu_B/172)^2)$, the deconfinement-transition line is $T = 201(1 - 0.0075(\mu_B/201)^2)$, the transition line determined from n/s is $T = 194(1 - 0.035(\mu_B/194)^2)$.

C. The EoS

In Sec. IIIB, we considered the transition line determined from $d\varepsilon/dT$, where $\varepsilon(T, \mu_B) = sT - P + \mu_B n$.

One uses the Tolman-Oppenheimer-Volkoff equations (TOV) equation to study structure of stars. The input EoS of the TOV equation is P and n . In addition, the isentropic trajectories, $n/s=\text{const}$, are important to study relativistic nuclear collisions. Therefore, we focus on P, s, ε, n .

In order to compare the present model with the previous model [21], we take the same assumption “ $f_H(T)$ has no μ_B dependence”, in the previous model. The resulting switching function $f_H^{\text{prev}}(T)$ is shifted to the left by about 10 MeV from $f_H(T)$ in Fig. 2. The difference between the present model with $f_H(T)$ and the previous model with $f_H^{\text{prev}}(T)$ shows EV effects. The previous model with $f_H^{\text{prev}}(T)$ is referred to as “HRG-HQH model” in this paper.

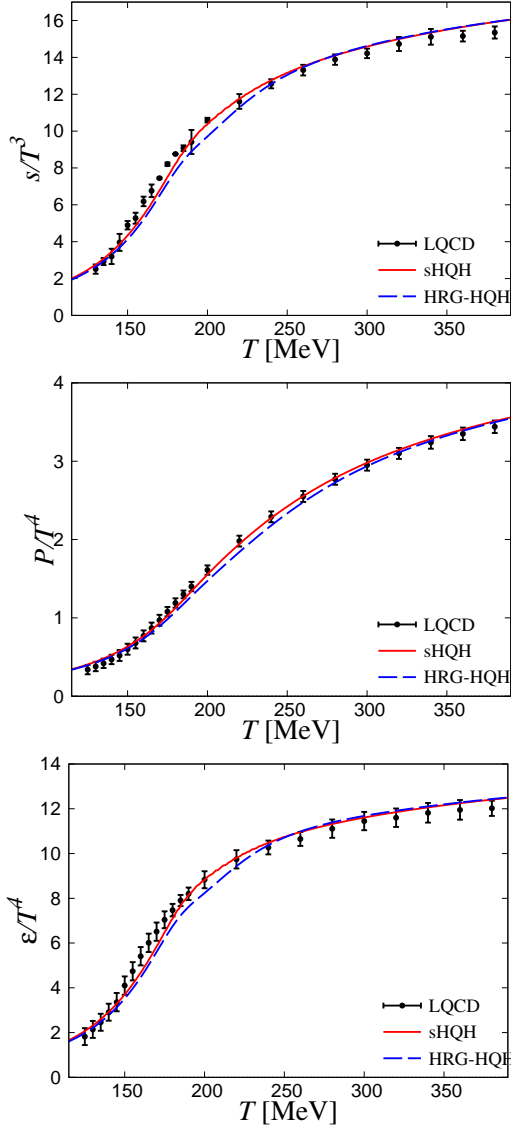


Fig. 8: T dependence of s, P, ε at $\mu_B = 0$ MeV. See the the text for the definition of lines. LQCD data are taken from Ref. [7].

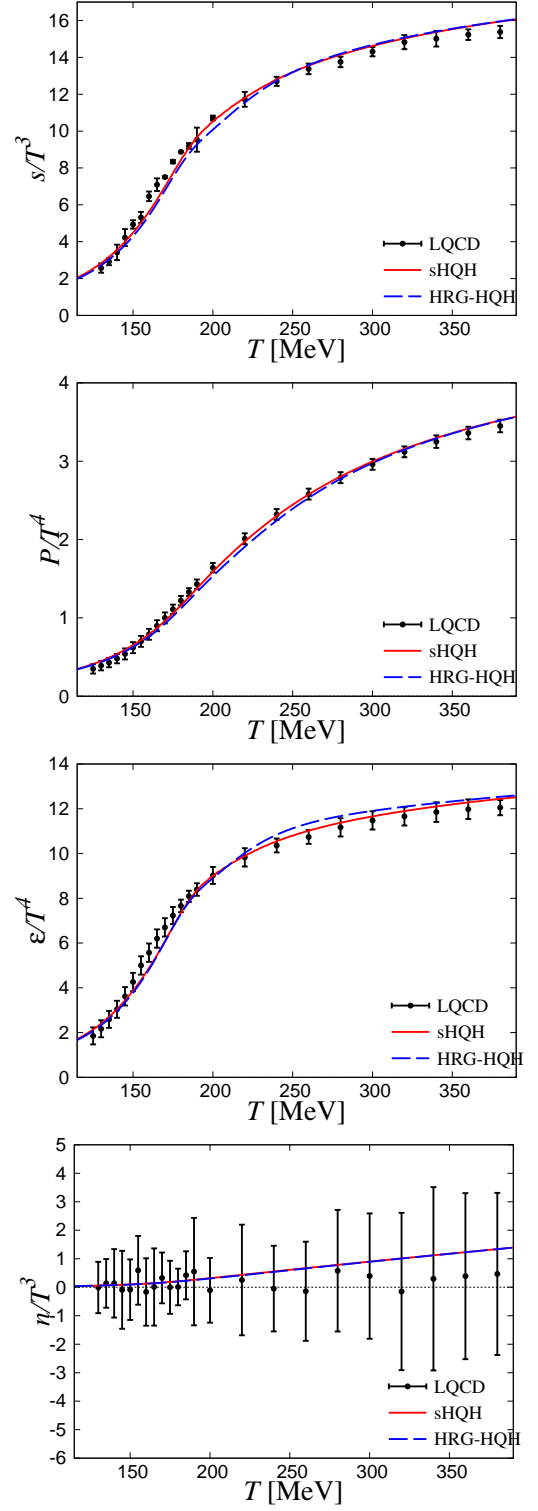


Fig. 9: T dependence of s, P, ε, n at $\mu_B = 100$ MeV. See the text for the definition of lines. LQCD data are taken from Ref. [7].

Figure 8 shows T dependence of s, P, ε , at $\mu_B = 0$ MeV. The solid and dashed lines are the results of sHQH and HRG-HQH models, respectively. Seeing $s(T)$, we find that the fitting of $f_H(T)$ is good, since the sHQH result agrees with LQCD data [7]. Also for P and ε , the sHQH model agree

with LQCD data. Comparing the results of sHQH and HRG-EV HQH models, we can find that EV effects are small for $\mu_B = 0$ MeV.

Figure 9 shows T dependence of s , P , ε , n at $\mu_B = 100$ MeV. The solid and dashed lines stand for the results of sHQH and HRG-HQH models, respectively. The s , P , ε , n of sHQH model reproduce LQCD data [7]. Comparing the two lines, we can see that EV effects are small still for $\mu_B = 100$ MeV.

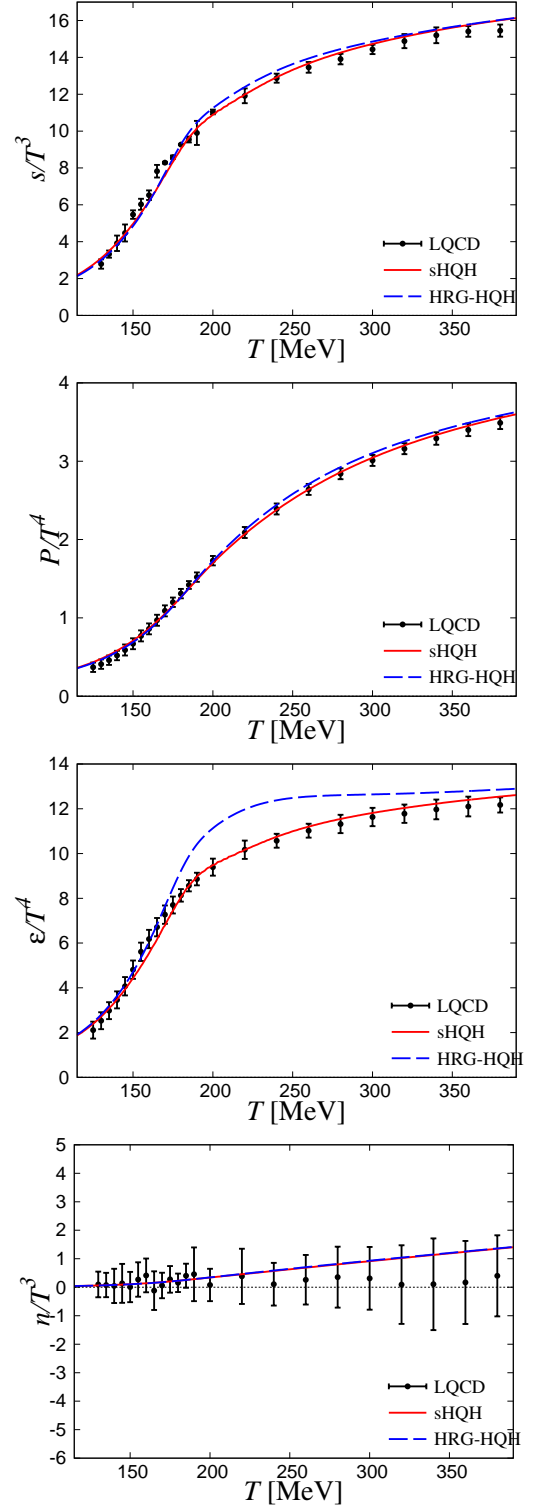


Fig. 10: T dependence of s , P , ε , n at $\mu_B = 200$ MeV. See the text for the definition of lines. LQCD data are taken from Ref. [7]; note that n is deduced from s , P , ε .

Figures. 10–12 shows T dependence of s , P , ε , n for $\mu_B = 200, 300, 400$ MeV. The results of sHQH model well reproduces the LQCD data [7]. EV effects become large as μ_B increases from 200 MeV to 400 MeV.

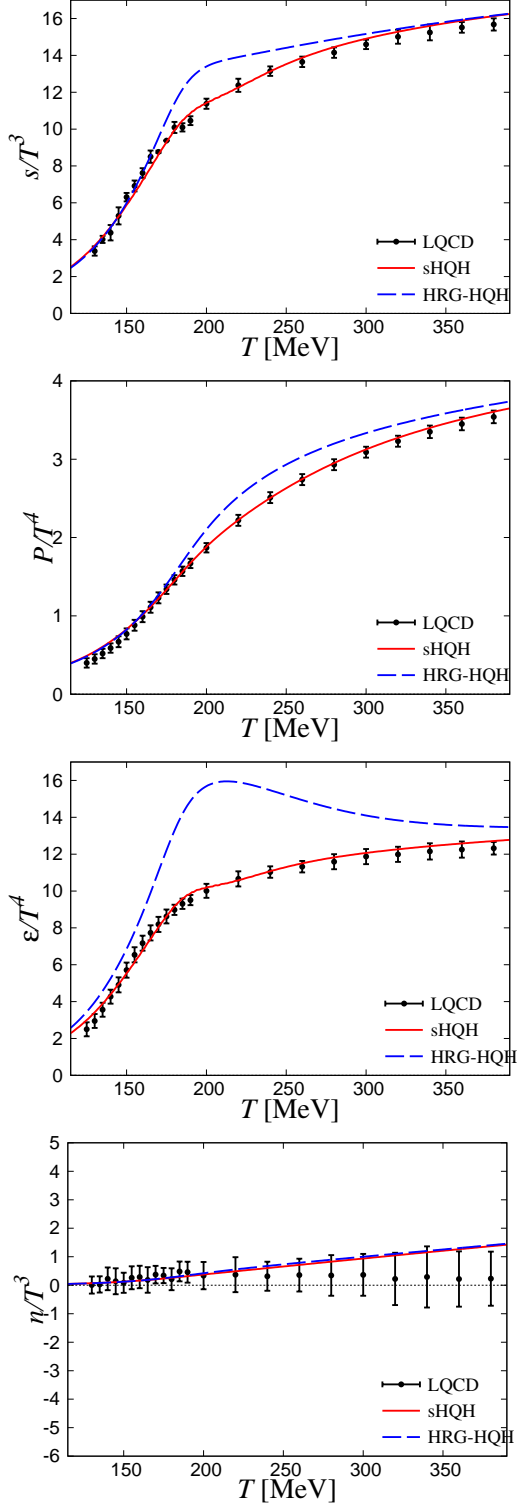


Fig. 11: T dependence of s, P, ε, n at $\mu_B = 300$ MeV. See the text for the definition of lines. LQCD are taken from Ref. [7]; note that n is deduced from s, P, ε .

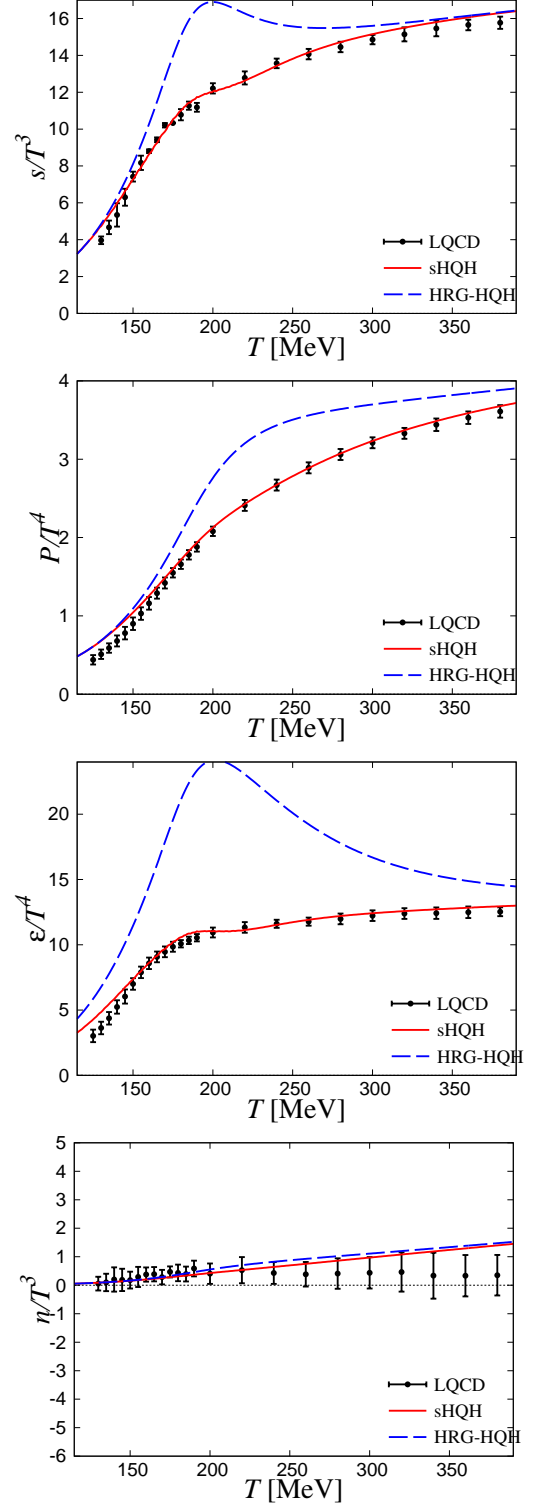


Fig. 12: T dependence of s, P, ε, n at $\mu_B = 400$ MeV. See the text for the definition of lines. LQCD are taken from Ref. [7]; note that n is deduced from s, P, ε .

IV. SUMMARY

We have improved the HQH model of Ref. [21], modifying the EV-HRG model [28, 29] for the hadron piece and using the simple IQ model for the quark-gluon piece. The modified EV-HRG model yields the baryon and antibaryon pressures as simple analytic functions of Eqs. (24)–(25), and ensures that the pressure is μ_B even.

We have determined the switching function f_H from s_{LQCD} at $\mu_B = 0$. The sHQH model with the switching function $f_H(T)$ well accounts for LQCD data on the Polyakov loop at $\mu_B = 0$ MeV. This makes it possible to predict the Polyakov loop for $\mu_B = 100, 200, 300, 400$ MeV. The EoS calculated with the sHQH model is successful in reproducing the corresponding LQCD data in $\mu_B \leq 400$ MeV, without introducing μ_B dependence to f_H , where the core radius $r = 0.335$ fm is taken. The switching function f_H has also a simple form, since it has no μ_B dependence.

As an interesting result of LQCD simulations for $\mu_B = 0$ [5], the peak position of $d\Delta_{l,s}/dT$ agrees with that of $d\varepsilon(T, \mu_B)/dT$. In LQCD simulations for finite μ_B [7], furthermore, a transition line is estimated by the peak of $d\varepsilon(T, \mu_B)/dT$. We can then guess that the transition region determined from ε is close to the chiral-transition region calculated with LQCD simulations. In fact, we show

that the transition region determined from $d\varepsilon(T, \mu_B)/dT$ almost agrees with the lattice result [8] on the chiral-transition region in $\mu_B \leq 400$ MeV. This may make it possible to define a chiral-transition region in μ_B – T plane with the peak and the half-value width of $d\varepsilon(T, \mu_B)/dT$.

As a deconfinement-transition region, we take the peak and the half-value width of $d\Phi(T, \mu_B)/dT$. As for the deconfinement transition, we predict the transition region and confirm that the deconfinement-transition line is above the transition line determined from $d\varepsilon(T, \mu_B)/dT$. In sHQH model, there is no evidence of attractor of isentropic trajectory. We have also found that the transition line determined from isentropic trajectories is between the deconfinement line and the transition line determined from $d\varepsilon(T, \mu_B)/dT$. The transition determined from isentropic trajectories may be deduced from relativistic nuclear collisions.

Acknowledgments

The authors thank Junpei Sugano and Takehiro Hirakida for useful contributions. H. K. is supported by Grant-in-Aid for Scientific Research (No.17K05446) from the Japan Society for the Promotion of Science (JSPS).

-
- [1] Y. Aoki, G. Endrödi, Z. Fodor, S. D. Katz and K. K. Szabó, *Nature* **443**, 675 (2006).
 - [2] Z. Fodor and S. D. Katz, *JHEP* **0404**, 050 (2004).
 - [3] Y. Aoki, A. Fodor, S. D. Katz, and K. K. Szabó, *Phys. Lett. B* **643**, 46 (2006).
 - [4] Y. Aoki, S. Borsanyi, S. Durr, Z. Fodor, S. D. Katz, S. Krieg and K. K. Szabo, *JHEP* **0906**, 088 (2009). doi:10.1088/1126-6708/2009/06/088 [arXiv:0903.4155 [hep-lat]].
 - [5] S. Borsanyi *et al.* [Wuppertal-Budapest Collaboration], *JHEP* **1009**, 073 (2010).
 - [6] G. Endrodi, Z. Fodor, S. D. Katz and K. K. Szabo, *JHEP* **1104**, 001 (2011).
 - [7] S. Borsanyi, G. Endrodi, Z. Fodor, S. D. Katz, S. Krieg, C. Ratti and K. K. Szabo, *JHEP* **1208**, 053 (2012).
 - [8] R. Bellwied, S. Borsanyi, Z. Fodor, J. Gunther, S. D. Katz, C. Ratti and K. K. Szabo, *Phys. Lett. B* **751**, 559 (2015).
 - [9] A. Bazavov *et al.*, *Phys. Rev. D* **95**, no. 5, 054504 (2017).
 - [10] S. Borsanyi, Z. Fodor, S. D. Katz, S. Krieg, C. Ratti, and K. K. Szabo, *JHEP* **01**, 138 (2012).
 - [11] S. Borsanyi, Z. Fodor, C. Hoelbling, S. D. Katz, S. Krieg and K. K. Szabo, *Phys. Lett. B* **730**, 99 (2014).
 - [12] A. Bazavov *et al.* [HotQCD Collaboration], *Phys. Rev. D* **90**, 094503 (2014).
 - [13] S. Borsanyi *et al.*, *Nature* **539**, 69 (2016).
 - [14] K. V. Olive *et al.* (Particle Data Group), *Chin. Phys. C* **38**, 090001 (2014).
 - [15] D. U. Jungnickel and C. Wetterich, *Phys. Rev. D* **53**, 5142 (1996) doi:10.1103/PhysRevD.53.5142 [hep-ph/9505267].
 - [16] M. Asakawa, T. Hatsuda, *Phys. Rev. D* **55**, 4488 (1997).
 - [17] C. Nonaka and M. Asakawa, *Phys. Rev. C* **71**, 044904 (2005) doi:10.1103/PhysRevC.71.044904 [nucl-th/0410078].
 - [18] M. Albright, J. Kapusta and C. Young, *Phys. Rev. C* **90**, 024915 (2014).
 - [19] M. Albright, J. Kapusta and C. Young, *Phys. Rev. C* **92**, 044904 (2015).
 - [20] A. Miyahara, Y. Torigoe, H. Kouno and M. Yahiro, *Phys. Rev. D* **94**, 016003 (2016).
 - [21] A. Miyahara, M. Ishii, H. Kouno and M. Yahiro, *Int. J. Mod. Phys. A* **32**, no. 36, 1750205 (2017).
 - [22] P. N. Meisinger, and M. C. Ogilvie, *Phys. Lett. B* **379**, 163 (1996).
 - [23] A. Dumitru, and R. D. Pisarski, *Phys. Rev. D* **66**, 096003 (2002).
 - [24] K. Fukushima, *Phys. Lett. B* **591**, 277 (2004); *Phys. Rev. D* **77**, 114028 (2008).
 - [25] Y. Sakai, K. Kashiwa, H. Kouno, and M. Yahiro, *Phys. Rev. D* **77**, 051901(R) (2008); *Phys. Rev. D* **78**, 036001 (2008).
 - [26] L. Landau and E. Lifshitz, *Statistical Physics* (Pergamon, New York, 1980).
 - [27] H. Kouno and F. Takagi, *Z. Phys.* **C45**, 43(1989).
 - [28] V. Vovchenko, D. V. Anchishkin and M. I. Gorenstein, *Phys. Rev. C* **91**, 024905 (2015).
 - [29] V. Vovchenko and H. Stocker, *J. Phys. G* **44**, 055103 (2017).
 - [30] V. Vovchenko, M. I. Gorenstein and H. Stoecker, *Phys. Rev. Lett.* **118**, 182301 (2017).